

Model Selection with Strong-lensing Systems

Kyle Leaf¹[★] and Fulvio Melia²[†]

¹*Department of Physics, The University of Arizona, AZ 85721, USA*

²*Department of Physics, The Applied Math Program, and Department of Astronomy, The University of Arizona, AZ 85721, USA*

ABSTRACT

In this paper, we use an unprecedentedly large sample (158) of confirmed strong lens systems for model selection, comparing five well studied Friedmann-Robertson-Walker cosmologies: Λ CDM, w CDM (the standard model with a variable dark-energy equation of state), the $R_h = ct$ universe, the (empty) Milne cosmology, and the classical Einstein-de Sitter (matter dominated) universe. We first use these sources to optimize the parameters in the standard model and show that they are consistent with *Planck*, though the quality of the best fit is not satisfactory. We demonstrate that this is likely due to under-reported errors, or to errors yet to be included in this kind of analysis. We suggest that the missing dispersion may be due to scatter about a pure single isothermal sphere (SIS) model that is often assumed for the mass distribution in these lenses. We then use the Bayes information criterion, with the inclusion of a suggested SIS dispersion, to calculate the relative likelihoods and ranking of these models, showing that Milne and Einstein-de Sitter are completely ruled out, while $R_h = ct$ is preferred over Λ CDM/ w CDM with a relative probability of $\sim 73\%$ versus $\sim 24\%$. The recently reported sample of new strong lens candidates by the Dark Energy Survey, if confirmed, may be able to demonstrate which of these two models is favoured over the other at a level exceeding 3σ .

Key words: cosmology: large-scale structure of the universe, cosmology: observations, cosmology: theory, distance scale; galaxies: general

[★] kyleaf@email.arizona.edu

[†] John Woodruff Simpson Fellow. E-mail: fmelia@email.arizona.edu

1 INTRODUCTION

With the continued discovery of new strong lensing systems, the gravitational bending of light is gaining in importance as a diagnostic tool for the expansion of the Universe. Einstein’s initial conclusion regarding the subject of gravitational lensing was that such a phenomenon would be very difficult to observe (Einstein 1936). It would take another sixty years before the first complete Einstein Ring was discovered (King et al. 1998). Strong gravitational lenses exist as uniquely geometrical phenomena, dependent only on the mass distribution of the nearer object and the distances between observer, lens, and source. Therefore, they offer a probe of the expansion history from the time the source emitted its light to the present day.

There has been a rapid progression in the number of known strongly lensed systems since the turn of the century, starting with The Lenses Structure and Dynamics (LSD) survey (Koopmans & Treu 2003; Treu & Koopmans 2002, 2004). Its successor, The Sloan Lens ACS (Advanced Camera for Surveys) (SLACS) found an additional 57 confirmed lenses (Bolton et al. 2008; Auger et al. 2009). Most recently, the SLACS survey has discovered an additional 40 lenses (Shu et al. 2017). The Baryon Oscillation Spectroscopic Survey (BOSS; Brownstein et al. 2012) produced another 25 confirmed strong galaxy-galaxy lenses, and the Strong Lensing Legacy Survey (SL2S; Gavazzi et al. 2014; Sonnenfeld et al. 2013a, 2013b), has resulted in a catalog of 31 confirmed lenses. Most recently, the Dark Energy Survey has compiled a catalog of 374 candidate systems (several of which were identified in prior surveys) awaiting follow-up observations for confirmation in the near future (Diehl et al. 2017). Combined, these surveys include lenses from redshifts $z = 0.06$ to 1, and sources from $z = 0.2$ to 3.6 (9 of them beyond $z = 3$). This rapid expansion in the catalog of available lens systems is crucial for cosmological work because the impact from the testing of cosmological models using these objects depends heavily on both the number of observations and the redshift range of the set.

In this paper, we use a catalog of 158 confirmed, strong lens systems suitable for testing various expansion scenarios—a significantly larger compilation than that of our previous analysis (Melia, Wei & Wu 2015) and that of Cao et al. (2015). We begin by constraining the properties of dark energy within w CDM (i.e., the standard model with a variable dark-energy equation of state), and then proceed to use model selection tools to determine which of several models is preferred by the strong-lens data. We consider the $R_h = ct$ universe, a Friedmann-Robertson-Walker (FRW) cosmology with zero active mass, i.e., $\rho + 3p = 0$, in terms of the total energy density ρ and

pressure p (Melia 2007, 2016, 2017a; Melia & Abdelqader 2009; Melia & Shevchuk 2012), the matter only Einstein-de-Sitter universe, and the empty Milne model (see, e.g., Vishwakarma 2013).

Our previous analysis (Melia, Wei, & Wu 2015) used a catalog of 69 sources and found that Λ CDM and $R_h = ct$ both performed reasonably well, though the number of measurements was insufficient to favor one model over the other. We also constructed a much larger mock catalog to estimate how many lensing systems would be required to carry out a definitive model selection, and concluded that a sample of several hundred lenses would suffice. The catalog of 158 systems we use here is approaching this threshold. But note that several of the 69 sources used in our previous study are not included here. In this paper, we restrict our attention to galaxy-galaxy lens systems, while some in the (Melia, Wei, & Wu 2015) analysis are of other types. When performing a comparison between the $R_h = ct$ universe and Λ CDM, however, it is important to recognize that these models make very similar predictions at low redshifts, meaning that the most important sources in this model selection are those at the highest redshifts. Unfortunately, the most recent additions from the SLACS survey (Shu et al. 2017) constitute only sources with a measured redshift $z \lesssim 1.3$. While these lenses are indeed useful for verifying the low-redshift predictions of any model, and for constraining the parameters of w CDM, they do not significantly contribute to the model selection itself. The SL2S and LSD surveys include all considered sources of redshift $z \gtrsim 1.6$, and therefore have the greatest impact on a direct comparison of the models. In § 2, we present the methods used to perform the fitting and model comparison. In § 3 we discuss the results of these calculations, and we end with a summary and our conclusions in § 4.

2 STRONG LENSING

Strong gravitational lensing has been used to constrain cosmological models in several recent publications, including Cao et al. (2012, 2015), Melia, Wei & Wu (2015), and An, Chang & Xu (2016). For a strongly lensed system with a single galaxy acting as the lens, the Einstein Radius depends only on three parameters: the angular diameter distances to the lens and source, and the mass distribution within the lensing galaxy. The most commonly used model for the lens galaxy's mass is a singular isothermal ellipsoid (SIE) (Ratnatunga, Griffiths & Ostrander 1999). Early-type galaxies (ellipticals) contain most of the cosmic stellar mass in the universe, and are therefore more commonly found as lenses than other types; approximating these as an ellipsoid is quite reasonable (Kochanek et al. 2000). The prior analyses by Cao et al. (2015) and Melia, Wei, & Wu (2015), however, reported consistency also with the simpler Singular Isothermal Sphere (SIS)

model (i.e., an SIE with zero ellipticity). The transparency of the results and the simplicity of the methodology therefore warrant making the SIS approximation. Nonetheless, to ensure that our results are not biased by this approach, we also consider potential random deviations from this simple model. An SIS determines the Einstein (angular) radius θ_E in terms of the 1-D velocity dispersion, σ_{SIS} , in the lensing galaxy. In terms of the ratio

$$\mathcal{D} = \frac{D_{ls}}{D_s}, \quad (1)$$

of the angular diameter distances D_{ls} and D_s between the lens and source, and source and observer, respectively, the Einstein radius is given as

$$\theta_E = 4\pi \frac{\sigma_{SIS}^2}{c^2} \mathcal{D}. \quad (2)$$

Note, however, that in place of σ_{SIS} , we follow the approach taken by Cao et al. (2015) in converting the observed velocity dispersion σ_{ap} measured within a given aperture and convert it to a velocity dispersion within a circular aperture of half the effective radius of the lens galaxy, with $\sigma_0 = \sigma_{ap}(\theta_{eff}/2\theta_{ap})^{-0.04}$, where θ_{eff} is the half-light radius of the lensing galaxy and θ_{ap} is the aperture size used to measure the velocity dispersion (Jørgensen, Franx & Kjaergaard 1995a, 1995b). The ratio \mathcal{D} therefore constitutes an observable quantity, written as

$$\mathcal{D}^{obs} = \frac{c^2 \theta_E}{4\pi \sigma_0^2}. \quad (3)$$

The quantity \mathcal{D} is well-defined for any given cosmology if the redshifts of the lens and source are known. In flat w CDM, we have

$$D(z_1, z_2) = \frac{c}{H_0} \frac{1}{1+z_2} \int_{z_1}^{z_2} \frac{dz'}{\sqrt{\Omega_m(1+z')^3 + \Omega_r(1+z')^4 + \Omega_{de}(1+z')^{3(1+w_{de})}}}, \quad (4)$$

where $w_{de} \equiv p_{de}/\rho_{de}$ is the dark-energy equation of state parameter, and Ω_i is today's density of species i in terms of the critical density $\rho_c \equiv 3c^2 H_0^2 / 8\pi G$. For our strong lens sample, Ω_r is negligible and may be ignored. For flatness, we also have $\Omega_m + \Omega_{de} = 1$, consistent with the latest *Planck* data release (Planck Collaboration 2016). This leaves only three free parameters, H_0 , w_{de} and Ω_m . When taking the ratio of two angular diameter distances, however, H_0 itself becomes irrelevant, so fitting the strong lens sample with w CDM reduces to an optimization based on only two free parameters.

We may use the same expression (Eq. 4) for the Einstein-De-Sitter universe, setting $\Omega_m=1$, $\Omega_r = 0$ and $\Omega_{de} = 0$. For the Milne universe, the corresponding expression is

$$D(z_1, z_2) = \frac{c}{H_0} \frac{1}{1+z_2} \sinh\left(\ln\left[\frac{1+z_2}{1+z_1}\right]\right) \quad (5)$$

(e.g., Vishwakarma 2015), while for the $R_h = ct$ model it is simply

$$D(z_1, z_2) = \frac{c}{H_0} \frac{1}{1+z_2} \ln \left[\frac{1+z_2}{1+z_1} \right] \quad (6)$$

(e.g., Melia, Wei & Wu 2015). The model predictions compared to the data are based on the expected ratio \mathcal{D}^{th} , defined in general as

$$\mathcal{D}^{\text{th}} = \frac{D(z_1, z_2)}{D(0, z_2)}. \quad (7)$$

For example, in the $R_h = ct$ universe, it is

$$\mathcal{D}^{\text{th}}(z_1, z_2) = 1 - \frac{\ln(1+z_1)}{\ln(1+z_2)}, \quad (8)$$

with corresponding expressions for the other cosmologies. Clearly, \mathcal{D} does not depend on H_0 for any of the considered models, removing all free parameters in $R_h = ct$, Milne, and Einstein-De-Sitter, while leaving w CDM with the two free parameters, w_{de} and Ω_m , for the optimization process. Note also that, by definition, this ratio is restricted to the range $0 \leq \mathcal{D} \leq 1$ for all lens systems.

3 DATA AND METHODOLOGY

Previous analyses of strong lenses used a variety of approaches to constrain the model parameters and for model selection (Melia, Wei, & Wu 2015; Cao et al. 2015; An, Chang & Xu 2016). For example, Cao et al. (2015) used a subset of the data we consider in this paper and several statistical features that warrant further consideration. In this paper, we compile a catalog of 158 confirmed sources (see Table 1), many identical to those included in Cao et al. (2015), but with the addition of 40 more discovered by SLACS (Shu et al. 2017). All redshifts are determined spectroscopically, and we use the Einstein Radii measured by the discovery teams based on fits to pixelized images of the sources. Cao et al. (2015) found that—assuming the *Planck* optimized value for Ω_m —the w CDM model is consistent to within 1σ with flat Λ CDM. Their fitting utilized the errors reported by the various surveys, in addition to assuming a uniform error of 5% for the measured Einstein Radius σ_{θ_E} (Grillo, Lombardi & Bertin, 2008). The expression for the combined error in \mathcal{D}^{obs} is then

$$\sigma_{\mathcal{D}} = \sqrt{4(\sigma_{\sigma_0})^2 + (\sigma_{\theta_E})^2}, \quad (9)$$

where σ_{σ_0} is the error reported for the velocity dispersion. Note that, while σ_0 does depend on the measured effective radius θ_{eff} , this is also determined to better than 5% accuracy, and the low power index of 0.04 (see expression following Eq. 2 above) results in an insignificant error contribution compared to that from the velocity dispersion itself.

Some lensing systems have two images, while others have four, a distinction that could generate some systematic differences between the two sub-groups. The previous analysis by Melia, Wei, & Wu (2015), however, showed that there are no significant differences between two-image and four-image systems. Given (i) that the recent SLACS data are not characterized in terms of which sub-group they belong to, and (ii) that there does not appear to be any dependence of the analysis on the number of images, we do not consider the two sub-samples separately here.

Table 1: Strong-lensing Systems

Name	z_l	z_s	σ_{ap} (km s ⁻¹)	θ_E (arcsec)	Survey	θ_{ap} (") (arcsec)	θ_{eff} (arcsec)	σ_0 (km s ⁻¹)
J0151+0049	0.517	1.364	219±39	0.68	BELLS	1.00	0.89	226±40
J0747+4448	0.437	0.897	281±52	0.61	BELLS	1.00	1.24	286±53
J0747+5055	0.438	0.898	328±60	0.75	BELLS	1.00	2.87	323±59
J0801+4727	0.483	1.518	98±24	0.49	BELLS	1.00	0.57	103±25
J0830+5116	0.530	1.332	268±36	1.14	BELLS	1.00	1.10	274±37
J0944-0147	0.539	1.179	204±34	0.72	BELLS	1.00	1.35	207±35
J1159-0007	0.579	1.346	165±41	0.68	BELLS	1.00	0.99	170±42
J1215+0047	0.642	1.297	262±45	1.37	BELLS	1.00	1.42	266±46
J1221+3806	0.535	1.284	187±48	0.70	BELLS	1.00	0.93	193±49
J1234-0241	0.490	1.016	122±31	0.53	BELLS	1.00	1.61	123±31
J1318-0104	0.659	1.396	177±27	0.68	BELLS	1.00	1.06	182±28
J1337+3620	0.564	1.182	225±35	1.39	BELLS	1.00	1.60	227±35
J1349+3612	0.440	0.893	178±18	0.75	BELLS	1.00	2.03	178±18
J1352+3216	0.463	1.034	161±21	1.82	BELLS	1.00	1.35	164±21
J1522+2910	0.555	1.311	166±27	0.74	BELLS	1.00	1.08	170±28
J1541+1812	0.560	1.113	174±24	0.64	BELLS	1.00	0.59	183±25
J1542+1629	0.352	1.023	210±16	1.04	BELLS	1.00	1.45	213±16
J1545+2748	0.522	1.289	250±37	1.21	BELLS	1.00	2.65	247±37
J1601+2138	0.544	1.446	207±36	0.86	BELLS	1.00	0.63	217±38
J1611+1705	0.477	1.211	109±23	0.58	BELLS	1.00	1.33	111±23
J1631+1854	0.408	1.086	272±14	1.63	BELLS	1.00	2.07	272±14

J1637+1439	0.391	0.874	208±30	0.65	BELLS	1.00	0.89	215±31
J2122+0409	0.626	1.452	324±56	1.58	BELLS	1.00	1.76	326±56
J2125+0411	0.363	0.978	247±17	1.20	BELLS	1.00	1.47	250±17
J2303+0037	0.458	0.936	274±31	1.02	BELLS	1.00	1.35	278±31
CFRS03-1077	0.938	2.941	251±19	1.24	LSD	1.25	1.60	256±19
HST-14176	0.810	3.399	224±15	1.41	LSD	1.25	1.06	232±16
HST-15433	0.497	2.092	116±10	0.36	LSD	1.25	0.41	125±11
MG-2016	1.004	3.263	328±32	1.56	LSD	0.65	0.31	347±34
Q0047-2808	0.485	3.595	229±15	1.34	LSD	1.25	0.82	239±16
J0212-0555	0.750	2.740	273±22	1.27	SL2S	0.90	1.22	277±22
J0213-0743	0.717	3.480	293±34	2.39	SL2S	1.00	1.97	293±34
J0214-0405	0.609	1.880	287±47	1.41	SL2S	1.00	1.21	293±48
J0217-0513	0.646	1.847	239±27	1.27	SL2S	1.50	0.73	253±29
J0219-0829	0.389	2.150	289±23	1.30	SL2S	1.00	0.95	298±24
J0223-0534	0.499	1.440	288±28	1.22	SL2S	1.00	1.31	293±28
J0225-0454	0.238	1.199	234±21	1.76	SL2S	1.00	2.12	233±21
J0226-0420	0.494	1.232	263±24	1.19	SL2S	1.00	0.84	272±25
J0232-0408	0.352	2.340	281±26	1.04	SL2S	1.00	1.14	287±27
J0848-0351	0.682	1.550	197±21	0.85	SL2S	0.90	0.45	208±22
J0849-0251	0.274	2.090	276±35	1.16	SL2S	0.90	1.34	279±35
J0849-0412	0.722	1.540	320±24	1.10	SL2S	0.90	0.46	338±25
J0850-0347	0.337	3.250	290±24	0.93	SL2S	0.70	0.28	309±26
J0855-0147	0.365	3.390	222±25	1.03	SL2S	0.70	0.69	228±26
J0855-0409	0.419	2.950	281±22	1.36	SL2S	0.70	1.13	283±22
J0904-0059	0.611	2.360	183±21	1.40	SL2S	0.90	2.00	182±21
J0959+0206	0.552	3.350	188±22	0.74	SL2S	0.90	0.46	199±23
J1359+5535	0.783	2.770	228±29	1.14	SL2S	1.00	1.13	233±30
J1404+5200	0.456	1.590	342±20	2.55	SL2S	1.00	2.03	342±20
J1405+5243	0.526	3.010	284±21	1.51	SL2S	1.00	0.83	294±22
J1406+5226	0.716	1.470	253±19	0.94	SL2S	1.00	0.80	262±20
J1411+5651	0.322	1.420	214±23	0.93	SL2S	1.00	0.85	221±24
J1420+5258	0.38	0.990	246±23	0.96	SL2S	1.00	1.11	252±24

J1420+5630	0.483	3.120	228±19	1.40	SL2S	1.00	1.62	230±19
J2203+0205	0.400	2.150	213±21	1.95	SL2S	1.00	0.99	219±22
J2205+0147	0.476	2.530	317±30	1.66	SL2S	0.90	0.66	330±31
J2213-0009	0.338	3.450	165±20	1.07	SL2S	1.00	0.27	179±22
J2219-0017	0.289	1.020	189±20	0.52	SL2S	0.70	1.01	191±20
J2220+0106	0.232	1.070	127±15	2.16	SL2S	1.00	0.80	132±16
J2221+0115	0.325	2.350	222±23	1.40	SL2S	1.00	1.12	227±24
J2222+0012	0.436	1.360	221±22	1.44	SL2S	1.00	1.56	223±22
J0008-0004	0.440	1.192	193±36	1.16	SLACS	1.50	1.71	197±37
J0029-0055	0.227	0.931	229±18	0.96	SLACS	1.50	2.16	232±18
J0037-0942	0.196	0.632	279±10	1.53	SLACS	1.50	2.19	283±10
J0044+0113	0.120	0.196	266±13	0.79	SLACS	1.50	2.61	267±13
J0109+1500	0.294	0.525	251±19	0.69	SLACS	1.50	1.38	259±20
J0157-0056	0.513	0.924	295±47	0.79	SLACS	1.50	1.06	308±49
J0216-0813	0.332	0.524	333±23	1.16	SLACS	1.50	2.67	335±23
J0252+0039	0.280	0.982	164±12	1.04	SLACS	1.50	1.39	169±12
J0330-0020	0.351	1.071	212±21	1.10	SLACS	1.50	1.20	220±22
J0405-0455	0.075	0.810	160±8	0.80	SLACS	1.50	1.36	165±8
J0728+3835	0.206	0.688	214±11	1.25	SLACS	1.50	1.78	219±11
J0737+3216	0.322	0.581	338±17	1.00	SLACS	1.50	2.82	339±17
J0808+4706	0.219	1.025	236±11	1.23	SLACS	1.50	2.42	238±11
J0822+2652	0.241	0.594	259±15	1.17	SLACS	1.50	1.82	264±15
J0841+3824	0.116	0.657	225±11	1.41	SLACS	1.50	4.21	222±11
J0903+4116	0.430	1.065	223±27	1.29	SLACS	1.50	1.78	228±28
J0912+0029	0.164	0.324	326±12	1.63	SLACS	1.50	3.87	323±12
J0935-0003	0.348	0.467	396±35	0.87	SLACS	1.50	4.24	391±35
J0936+0913	0.190	0.588	243±12	1.09	SLACS	1.50	2.11	246±12
J0946+1006	0.222	0.608	263±21	1.38	SLACS	1.50	2.35	266±21
J0956+5100	0.240	0.470	334±17	1.33	SLACS	1.50	2.19	338±17
J0959+0410	0.126	0.535	197±13	0.99	SLACS	1.50	1.39	203±13
J1016+3859	0.168	0.439	247±13	1.09	SLACS	1.50	1.46	254±13
J1020+1122	0.282	0.553	282±18	1.20	SLACS	1.50	1.59	289±18

J1023+4230	0.191	0.696	242±15	1.41	SLACS	1.50	1.77	247±15
J1100+5329	0.317	0.858	187±23	1.52	SLACS	1.50	2.24	189±23
J1106+5228	0.096	0.407	262±13	1.23	SLACS	1.50	1.68	268±13
J1112+0826	0.273	0.630	320±20	1.49	SLACS	1.50	1.50	329±21
J1134+6027	0.153	0.474	239±12	1.10	SLACS	1.50	2.02	243±12
J1142+1001	0.222	0.504	221±22	0.98	SLACS	1.50	1.91	225±22
J1143-0144	0.106	0.402	269±13	1.68	SLACS	1.50	4.80	264±13
J1153+4612	0.180	0.875	226±15	1.05	SLACS	1.50	1.16	235±16
J1204+0358	0.164	0.631	267±17	1.31	SLACS	1.50	1.47	275±17
J1205+4910	0.215	0.481	281±14	1.22	SLACS	1.50	2.59	283±14
J1213+6708	0.123	0.640	292±15	1.42	SLACS	1.50	3.23	291±15
J1218+0830	0.135	0.717	219±11	1.45	SLACS	1.50	3.18	218±11
J1250+0523	0.232	0.795	252±14	1.13	SLACS	1.50	1.81	257±14
J1251-0208	0.224	0.784	233±23	0.84	SLACS	1.50	2.61	234±23
J1330-0148	0.081	0.712	185±9	0.87	SLACS	1.50	0.89	194±9
J1402+6321	0.205	0.481	267±17	1.35	SLACS	1.50	2.70	268±17
J1403+0006	0.189	0.473	213±17	0.83	SLACS	1.50	1.46	219±17
J1416+5136	0.299	0.811	240±25	1.37	SLACS	1.50	1.43	247±26
J1430+4105	0.285	0.575	322±32	1.52	SLACS	1.50	2.55	324±32
J1436-0000	0.285	0.805	224±17	1.12	SLACS	1.50	2.24	227±17
J1451-0239	0.125	0.520	223±14	1.04	SLACS	1.50	2.48	225±14
J1525+3327	0.358	0.717	264±26	1.31	SLACS	1.50	2.90	264±26
J1531-0105	0.160	0.744	279±14	1.71	SLACS	1.50	2.50	281±14
J1538+5817	0.143	0.531	189±12	1.00	SLACS	1.50	1.58	194±12
J1621+3931	0.245	0.602	236±20	1.29	SLACS	1.50	2.14	239±20
J1627-0053	0.208	0.524	290±14	1.23	SLACS	1.50	1.98	295±14
J1630+4520	0.248	0.793	276±16	1.78	SLACS	1.50	1.96	281±16
J1636+4707	0.228	0.674	231±15	1.09	SLACS	1.50	1.68	236±15
J2238-0754	0.137	0.713	198±11	1.27	SLACS	1.50	2.33	200±11
J2300+0022	0.228	0.464	279±17	1.24	SLACS	1.50	1.83	285±17
J2303+1422	0.155	0.517	255±16	1.62	SLACS	1.50	3.28	254±16
J2321-0939	0.082	0.532	249±8	1.60	SLACS	1.50	4.11	246±8

J2341+0000	0.186	0.807	207±13	1.44	SLACS	1.50	3.15	207±13
J0143-1006	0.221	1.1046	203±17	1.23	SLACS2017	1.50	3.24	202±17
J0159-0006	0.1584	0.7477	216±18	0.92	SLACS2017	1.50	1.58	222±18
J0324+0045	0.321	0.9199	183±19	0.55	SLACS2017	1.50	1.67	187±19
J0324-0110	0.4456	0.6239	310±38	0.63	SLACS2017	1.50	2.23	314±38
J0753+3416	0.1371	0.9628	208±12	1.23	SLACS2017	1.50	1.89	212±12
J0754+1927	0.1534	0.7401	193±16	1.04	SLACS2017	1.50	1.46	199±16
J0757+1956	0.1206	0.8326	206±11	1.62	SLACS2017	1.50	3.67	204±11
J0826+5630	0.1318	1.2907	163±8	1.01	SLACS2017	1.50	1.64	167±8
J0847+2348	0.1551	0.5327	199±16	0.96	SLACS2017	1.50	1.54	204±16
J0851+0505	0.1276	0.6371	175±11	0.91	SLACS2017	1.50	1.35	181±11
J0920+3028	0.2881	0.3918	297±17	0.70	SLACS2017	1.50	4.25	293±17
J0955+3014	0.3214	0.4671	271±33	0.54	SLACS2017	1.50	2.95	271±33
J0956+5539	0.1959	0.8483	188±11	1.17	SLACS2017	1.50	1.96	191±11
J1010+3124	0.1668	0.4245	221±11	1.14	SLACS2017	1.50	3.26	220±11
J1031+3026	0.1671	0.7469	197±13	0.88	SLACS2017	1.50	1.04	206±14
J1040+3626	0.1225	0.2846	186±10	0.59	SLACS2017	1.50	1.30	192±10
J1041+0112	0.1006	0.2172	200±7	0.60	SLACS2017	1.50	2.50	201±7
J1048+1313	0.133	0.6679	195±10	1.18	SLACS2017	1.50	1.90	199±10
J1051+4439	0.1634	0.538	216±16	0.99	SLACS2017	1.50	1.66	221±16
J1056+4141	0.1343	0.8318	157±10	0.72	SLACS2017	1.50	1.81	160±10
J1101+1523	0.178	0.5169	270±15	1.18	SLACS2017	1.50	0.89	283±16
J1116+0729	0.1697	0.686	190±11	0.82	SLACS2017	1.50	2.44	192±11
J1127+2312	0.1303	0.361	230±9	1.25	SLACS2017	1.50	2.69	231±9
J1137+1818	0.1241	0.4627	222±8	1.29	SLACS2017	1.50	1.79	227±8
J1142+2509	0.164	0.6595	159±10	0.79	SLACS2017	1.50	1.51	163±10
J1144+0436	0.1036	0.2551	207±14	0.76	SLACS2017	1.50	1.22	215±15
J1213+2930	0.0906	0.5954	232±7	1.35	SLACS2017	1.50	1.73	237±7
J1301+0834	0.0902	0.5331	178±8	1.00	SLACS2017	1.50	1.25	184±8
J1330+1750	0.2074	0.3717	250±12	1.01	SLACS2017	1.50	2.85	251±12
J1403+3309	0.0625	0.772	190±6	1.02	SLACS2017	1.50	2.00	193±6
J1430+6104	0.1688	0.6537	180±15	1.00	SLACS2017	1.50	2.24	182±15

J1433+2835	0.0912	0.4115	230±6	1.53	SLACS2017	1.50	3.23	229±6
J1541+3642	0.1406	0.7389	194±11	1.17	SLACS2017	1.50	1.55	199±11
J1543+2202	0.2681	0.3966	285±16	0.78	SLACS2017	1.50	2.32	288±16
J1550+2020	0.1351	0.3501	243±9	1.01	SLACS2017	1.50	1.68	249±9
J1553+3004	0.1604	0.5663	194±15	0.84	SLACS2017	1.50	2.15	197±15
J1607+2147	0.2089	0.4865	197±16	0.57	SLACS2017	1.50	2.63	198±16
J1633+1441	0.1281	0.5804	231±9	1.39	SLACS2017	1.50	2.39	233±9
J2309-0039	0.2905	1.0048	184±13	1.14	SLACS2017	1.50	2.08	187±13
J2324+0105	0.1899	0.2775	245±15	0.59	SLACS2017	1.50	1.10	255±16

Let us now describe the sequence of steps taken to minimize the overall scatter in the data. If we simply use the full set of 158 confirmed sources, without the introduction of an additional dispersion associated with the SIS and the exclusion of outliers, we find that *Planck* Λ CDM (with $\Omega_m = 0.308$, $\Omega_{de} \equiv \Omega_\Lambda = 1 - \Omega_m$) fits the strong lenses with a reduced χ^2_{dof} (χ^2 per degree of freedom) of $\simeq 2.7$, which is not satisfactory. A more serious issue is that most of the data—89 out of 158 sources—are inconsistent with Planck Λ CDM at more than 1σ . By comparison, if the reported errors were truly Gaussian, we should expect ≈ 50 of the 158 measurements to deviate by more than 1σ from an accurate cosmological model. But there are clearly several mitigating circumstances. For example, in our initial analysis, we find that a single source, J0850-0347, deviates by more than 5σ from all the considered models, and we therefore exclude it as a significant outlier from all further consideration. With this single source excluded, the χ^2_{dof} for *Planck* Λ CDM immediately drops to $\simeq 2.4$.

This improvement notwithstanding, such a poor χ^2_{dof} contrasts sharply with the outcome reported in Melia, Wei & Wu (2015), but we note that an additional error term, σ_f , was included in that earlier paper to characterize possible random deviations from the simple isothermal sphere (SIS) model. This dispersion was assumed to be 6%, resulting in a 12% contribution to σ_D based on standard error propagation. Nonetheless, were we to include that additional scatter here, the resulting $\chi^2_{\text{dof}} \simeq 1.5$ for the *Planck* Λ CDM best fit would still be significantly greater than the value (i.e., $\chi^2_{\text{dof}} \simeq 1.2$) found in our previous work. The difference is entirely due to the new data we have

added to the sample in this paper, at least some of which appear to deviate significantly from the *Planck* model.

We believe that contributing factors to this disparity are (i) that the reported errors are possibly underestimated, and (ii) that there is an additional unrecognized systematic effect that has yet to be included in the analysis. In addition, we carefully excluded from our previous analysis those lens systems with $\mathcal{D}^{\text{obs}} > 1$, which are unphysical (see Eq. 8). If we follow the same steps here with the larger sample, introducing the additional SIS dispersion and excluding the 28 lenses with $\mathcal{D}^{\text{obs}} > 1$, 11 of which are from the 2017 SLACS catalog, and also exclude the aforementioned extreme outlier J0850-0347, we find that $\chi^2_{\text{dof}} \approx 1.01$ for the *Planck* Λ CDM cosmology, nearly identical to our previous result. As we explain in more detail below, there are good reasons for believing that the SIS dispersion may be bigger than the value we used previously. For example, in their fitting, Cao et al. (2012) invoked possible deviations from SIS contributing a scatter of up to 20%. This appears to be more in line with our preliminary finding here, so we investigate the impact of such a large dispersion on our optimization of the parameters in the w CDM cosmology.

We use maximization of the likelihood function to constrain and compare the models, including w CDM. We calculate \mathcal{D}^{obs} using Equation (3), and \mathcal{D}^{th} using Equation (7). For each measurement of \mathcal{D}^{obs} we also determine the corresponding error through standard error propagation, in which

$$\sigma_{\mathcal{D}^{\text{obs}}} = \mathcal{D}^{\text{obs}} \sqrt{\left(\frac{\sigma_{\theta_E}}{\theta_E}\right)^2 + \left(\frac{2\sigma_{\sigma_0}}{\sigma_0}\right)^2 + \sigma_X^2}, \quad (10)$$

where σ_X is a unitless composite error term comprising the scatter about the SIS average and any other source of scatter in the measurements. We iterate the value of σ_X (described below), while also systematically eliminating sources with a \mathcal{D}^{obs} exceeding 1, since these are clearly unphysical, and we also exclude J0850-0347, which is an extreme outlier in every model we tested.

In the method of maximum likelihood estimation (MLE; Wei et al. 2015a), the joint likelihood function for all parameters, based on a flat Bayesian prior, is

$$\mathcal{L} = \prod_i \frac{1}{\sqrt{2\pi} \sigma_{\mathcal{D}_i}} \exp\left[-\frac{\chi_i^2}{2}\right] \quad (11)$$

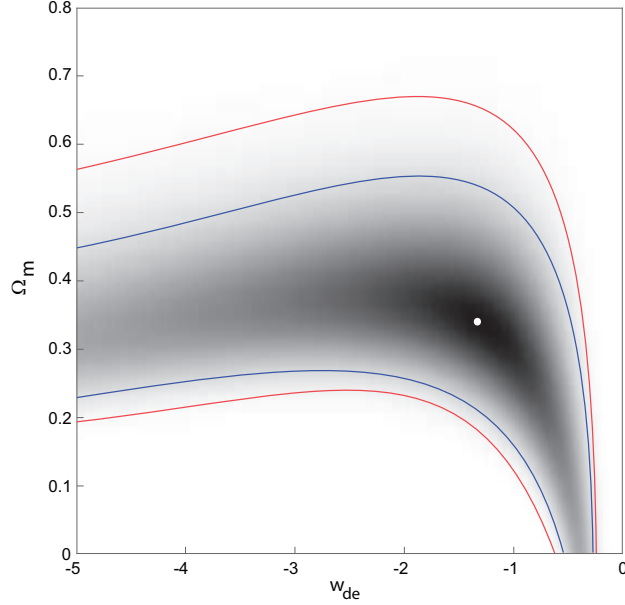
where, for each measurement,

$$\chi_i^2 \equiv \frac{(\mathcal{D}_i^{\text{obs}} - \mathcal{D}_i^{\text{th}})^2}{\sigma_{\mathcal{D},i}^2}. \quad (12)$$

The iteration on σ_X ends when the optimization of w CDM results in a $\chi^2_{\text{dof}} = 1$. Once σ_X has been identified in this way, we use the same value for all the models in order to keep the comparison as transparent as possible. Although this approach tends to favour w CDM somewhat, we will see

Table 2. Best-fitting Parameters for the CDM models (Constrained by $\mathcal{D}^{\text{obs}} \leq 1$)

Model	Ω_m	w_{de}	σ_X	χ^2_{dof}
$w\text{CDM}$	$0.33^{+0.13}_{-0.15}$	$-1.29^{+0.97}_{-6.09}$	12.2%	0.998
ΛCDM	$0.29^{+0.12}_{-0.08}$	-1 (Fixed)	12.2%	0.999

**Figure 1.** Probability density plot in the $\Omega_m - w_{\text{de}}$ plane for $w\text{CDM}$. The contours give the 1σ and 2σ (i.e., the 68% and 95%) confidence regions for the optimized parameters in $w\text{CDM}$. The white dot shows the best fit values.

that it does not influence the model ranking significantly. For example, the disfavoured models are rejected strongly and, clearly, changing σ_X by a few percentage points will not alter this outcome.

The resulting best-fit values (including σ_X), calculated via the marginal probability of each parameter, are reported in Table 2 for both $w\text{CDM}$ and ΛCDM . The latter has one fewer parameter (since $w_{\text{de}} = -1$). The corresponding 1σ and 2σ confidence contours for $w\text{CDM}$ in the $\Omega_m - w_{\text{de}}$ plane, along with the overall probability density, are shown in fig. 1. Retaining only sources with $\mathcal{D}^{\text{obs}} \leq 1$ reduces our overall sample size from 157 (excluding the extreme outlier) to 129 lenses, but it also decreases the magnitude of σ_X compared to what it would have been for the entire sample. A quick inspection of Table 2 shows that the steps we have taken in identifying the final sample for model selection produces results that are consistent with the *Planck* measurements. Both Ω_m and w_{de} are fully consistent with the parameter values in the concordance model, particularly in the case of ΛCDM .

Table 3. Model Comparisons and Ranking (based on 129 lenses with the constraint $\mathcal{D}^{obs} \leq 1$)

Model	χ^2_{dof}	BIC	Relative Likelihood
$R_h = ct$	1.020	131.559	73.032%
ΛCDM	0.999	133.748	24.443%
$w\text{CDM}$	0.998	138.484	2.290%
Milne	1.109	143.063	0.232%
EdS	1.194	151.314	$3.75 \times 10^{-3}\%$

With the best-fitting parameters for flat $w\text{CDM}$ thus determined, we now proceed to carry out model selection based on the Bayes information criterion (BIC; Schwarz 1978; Melia & Maier 2013; Wei et al. 2015b). The BIC is defined as

$$\text{BIC} = -2\mathcal{L} + n \ln(N) , \quad (13)$$

where \mathcal{L} is the likelihood in Equation (11), N is the number of measurements in the final reduced sample, here 129, and n is the number of free parameters. In this application, $w\text{CDM}$ is penalized with $n = 2$, and ΛCDM with $n = 1$, while $R_h = ct$, Milne, and Einstein-de-Sitter each have $n = 0$ (no free parameters). When comparing cosmologies using the BIC, the probability that a specific model \mathcal{M}_α is the correct one among the set being considered is

$$P(\mathcal{M}_\alpha) = \frac{\exp(-\text{BIC}_\alpha/2)}{\sum_i \exp(-\text{BIC}_i/2)} . \quad (14)$$

Table 3 summarizes the χ^2_{dof} , the BIC, and *relative* likelihood (calculated from Eq. 14) of each model in this comparison.

4 DISCUSSION

Our analysis in this paper affirms the important role played by strong lenses in helping to refine the parameters in the standard model and, perhaps more importantly going forward, providing ample confirmation, if not definitive evidence, in model selection. Previous work by Melia, Wei & Wu (2015) and Cao et al. (2015), albeit with smaller samples, suggested that—while individual lenses may deviate from an SIS model—the statistics of a large sample appears to be consistent with this simple internal structure of the lens’s mass distribution. We have therefore adopted this approach to update the optimization of parameters in the standard model based on fits to the strong lens angular diameter distance dependence on redshift, and then to compare the predictions of $w\text{CDM}$ with those of four other cosmologies. We have found, however, that ignoring individual variations from a pure SIS structure results in an unsatisfactory fit using $w\text{CDM}$ and ΛCDM , necessitating

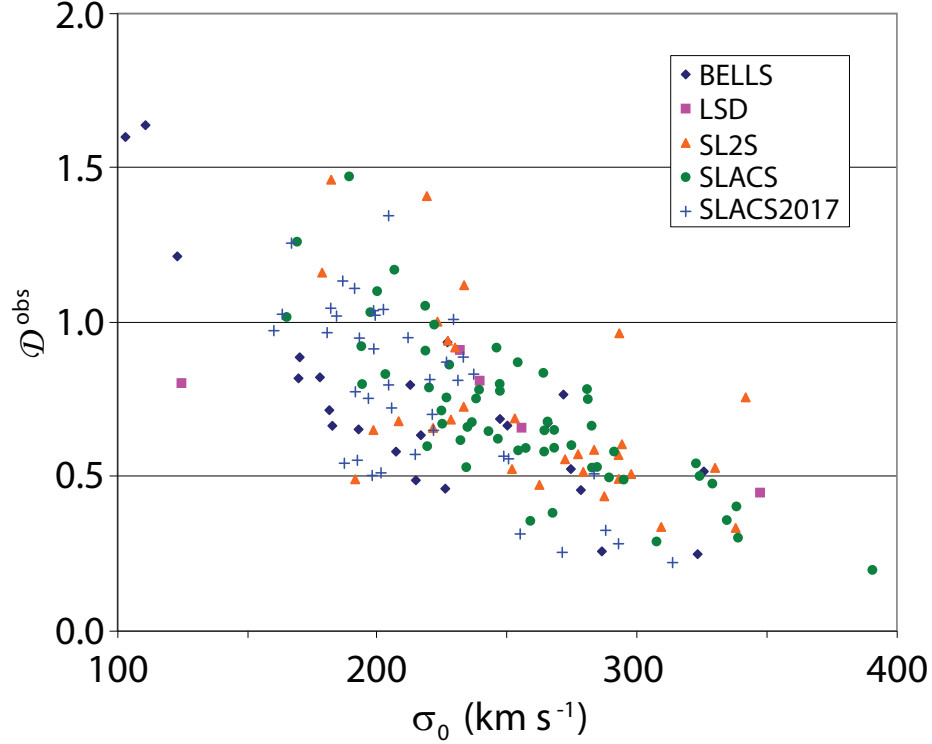


Figure 2. An apparent bias in the measured ratio \mathcal{D}^{obs} with increasing velocity dispersion σ_0 . This trend exceeds the dependence of \mathcal{D}^{obs} on σ_0 expected from Eq. (3), in which θ_E ought to change in concert with σ_0 to largely offset such a correlation. Two outliers, J2220+0106 and J1352+3216, lie outside this plot due to their extreme \mathcal{D}^{obs} values of 4.32 and 2.36, respectively.

the introduction of a dispersion to represent the scatter associated with this over-simplified lens model.

It is important to emphasize that our sample is larger than that used in any previous attempt to carry out this type of analysis, and that it includes all of the sources used by Cao et al. (2015) (with the exception of a single outlier). We have supplemented this catalog with the 40 recently confirmed lenses uncovered with SLACS (Shu et al. 2017). Our best-fit parameters for the standard model are consistent with those of *Planck*, but based solely on the reported errors, the reduced χ^2_{dof} for the optimized model is unacceptably large, unless we include the aforementioned additional scatter in the analysis. We argue that either the errors have been under-reported, or that the additional dispersion cannot be ignored with observations such as these. We have therefore sought to identify its magnitude, representing deviations from a pure homogeneous SIS model for all the lenses. Note, however, that our inferred uncertainty on the optimized value of w_{de} (in the case of w CDM) is larger than that obtained by Cao et al. (2015), in spite of the larger lens catalog at our disposal.

But though the introduction of the dispersion σ_X to account for individual departures from a pure SIS lens structure has greatly reduced the scatter about the best-fit model in w CDM/ Λ CDM,

the problems with using such a simple lens have not been completely eliminated, as demonstrated in fig. 2. Cao et al. (2015) reported a significant trend in deviations from their fitted cosmological model as a function of σ_0 . We find the same trend with the larger sample used in this paper, in which \mathcal{D}^{obs} decreases faster than expected from Eq. (3) with increasing σ_0 . Certainly Eq. (3) predicts that for a fixed θ_E , one should see such a trend. But the Einstein radius also depends on the lens galaxy's mass distribution and the distance ratio between the lens and source objects, which should largely offset the trend seen in fig. 2. There is no reason to expect a significant correlation between the mass distribution of the lensing object and the distance ratio between it and the source galaxy, as these are two independent parameters that produce the Einstein ring. For this reason, such a significant correlation between \mathcal{D}^{obs} and σ_0 can be taken as some evidence that the simple SIS galaxy mass distribution model is not robust enough to accurately account for all the individual variations seen from source to source.

In the redshift range of these data, the best-fit w CDM, Λ CDM and $R_h = ct$ models predict comparable \mathcal{D}^{th} ratios. In each case, strongly lensed systems with $\sigma_0 \lesssim 250 \text{ km s}^{-1}$ generally have $\mathcal{D}^{\text{obs}} > \mathcal{D}^{\text{th}}$, but this trend is reversed for $\sigma_0 \gtrsim 250 \text{ km s}^{-1}$. The effect tends to get bigger as σ_0 increases or decreases away from its median value $\sim 233 \text{ km s}^{-1}$. In fact, all lens systems with an unphysical $\mathcal{D}^{\text{obs}} > 1$ have $\sigma_0 \lesssim 233 \text{ km s}^{-1}$. Working with a smaller sample of the data than we have here, Cao et al. (2015) attempted to generalize the SIS model by characterizing it as a spherically symmetric power-law mass distribution of the form $\rho \sim r^{-\gamma}$. Their optimized value of γ was consistent with -2 , however, which is in fact the SIS model, but they also noticed large deviations from their fits for σ_0 very different from 250 km s^{-1} . One should therefore be cautious with the use of an SIS model in future attempts to constrain or compare cosmologies using strong lensing data. At a minimum, one should carefully study the impact of a density profile varying with changing σ_0 .

A principal goal of this paper has been to significantly update the results of Melia, Wei & Wu (2015). In that analysis, with only 69 strong lenses, no significant preference was determined for either Λ CDM or $R_h = ct$. Based on a much larger sample of mock data, however, these authors concluded that approximately 200 lenses would be required to show that Λ CDM is preferred over $R_h = ct$ at the 99.7% confidence level if the standard model is the correct description of nature. On the flip side, this earlier work also showed that about 300 lenses would be needed to demonstrate the superiority of $R_h = ct$ over Λ CDM at a comparable level of confidence if it turned out that the former was the correct model. With the 158 systems we have considered here, reduced to 129 with the exclusion of the unphysical ones, our sample has not quite reached that size yet, but we are

rapidly approaching these thresholds. As Table 3 shows, the current status has the $R_h = ct$ universe as the preferred model, followed by Λ CDM, which is favoured over w CDM. Although w CDM is slightly more flexible in fitting the data than Λ CDM, the penalty incurred by the additional free parameter causes it to be favoured less than the standard model with a fixed dark-energy equation of state. At the same time, these results show that the Milne universe and Einstein-de Sitter are completely ruled out. The sample of strong lenses now available for model selection is therefore already large enough to provide results consistent with those of many other kinds of observation, all of which have thus far tended to favour $R_h = ct$ over w CDM/ Λ CDM (see, e.g., Melia 2013a, 2013b; and especially Table 1 in Melia 2017b).

5 CONCLUSION

An important byproduct of this analysis has been our assessment of the likely intrinsic scatter associated with the SIS model for the lens. If the random variation in galaxy morphology is almost Gaussian, we find that an additional error term of about 12.22% is necessary to have 68% of the observations lie within 1σ of the best-fit w CDM model. This factor is smaller than—though consistent with—the 20% scatter suggested by Cao et al. (2012). Thus, in spite of the fact that our sample here is twice as large as that used in our previous analysis (Melia, Wei & Wu 2015), our conclusion regarding the size of this scatter is virtually identical to that of our previous work, in which we found that $\sigma_X \sim 0.12$. Interestingly, this is very close to the conclusion drawn earlier by Treu et al. (2006), who also argued for the inclusion of a scatter of about 12%. But this is only true when sources with $\mathcal{D}^{\text{obs}} > 1$ are excluded. Were we to include all 157 sources (the complete sample of 158 minus the significant outlier J0850-0347), we would find that σ_X is closer to 18%. As noted, this difference provides some evidence that the SIS lens model breaks down for the more extreme values of σ_0 .

Based on our earlier work (Melia, Wei & Wu 2015) and the significant improvement we have seen using a much bigger sample in this paper, we are certain that strong lenses will play a pivotal role in model selection going forward—but preferably with an improved model for the lens mass. Already DES has released a catalog of 348 new strong lens candidates (Diehl et al. 2017). Spectroscopic follow-up observations are anticipated over the next several years. Even if only half of these are verified lenses, with a sufficient number of sources at $z > 3$, we anticipate that the next update of our analysis may offer an even stronger answer as to whether $R_h = ct$ or Λ CDM is the correct cosmology.

ACKNOWLEDGMENTS

We are grateful to Joel Brownstein, Raphel Gavazzi, and Tommaso Treu for their correspondence and helpful suggestions, and to the anonymous referee for a very helpful and thoughtful review. FM is supported by the Chinese Academy of Sciences Visiting Professorships for Senior International Scientists under grant 2012T1J0011, and the Chinese State Administration of Foreign Experts Affairs under grant GDJ20120491013.

REFERENCES

- Auger M. W., Treu T., Bolton A. S., Gavazzi R., Koopmans L. V. E., Marshall P. J., Bundy K., Moustakas L. A., 2009, *ApJ*, 705, 1099
- An J., Chang B., Xu L., 2016 *Chinese Phys. Lett.* 33, 079801
- Bolton A. S., Burles S., Koopmans L. V. E., Treu T., Gavazzi R., Moustakas L. A., Wayth R., Schlegel D. J., 2008, *ApJ*, 682, 964
- Brownstein J. R. et al. 2012, *Apj*, 744, 41
- Cao S., Pan Y., Biesiada M., Godlowski W., Zhu Z-H., 2012a, *J. Cosmology Astropart. Phys.*, 3, 016
- Cao S., Biesiada M., Gavazzi R., Piórkowska A., Zhu Z.-H., 2015, *ApJ*, 806, 185
- Diehl H. T. et al., 2017, *ApJS*, 232, 15
- Einstein A., 1936, *Sci*, 84, 506
- Gavazzi R., Marshall P. J., Treu T., Sonnenfeld A., 2014, *ApJ*, 785, 144
- Grillo C., Lombardi M., Bertin G., 2008, *A&A*, 477, 397
- Jørgensen I., Franx M., Kjaergaard P., 1995a, *MNRAS*, 273, 1097
- Jørgensen I., Franx M., Kjaergaard P., 1995b, *MNRAS*, 276, 1341
- King, L. J., Jackson, N., Blandford, R. D., Bremer, M. N., Browne, I. W. A., de Bruyn, A. G., 1998, *MNRAS*, 295, L41
- Kochanek C. S. et al., 2000, *ApJ*, 543, 131
- Koopmans L. V. E., Treu T., 2003, *ApJ*, 583, 137
- Melia F., 2007, *MNRAS*, 382, 1917
- Melia F., 2013a, *A&A*, 553, A76
- Melia, F., 2013b, *ApJ*, 764, id.72
- Melia, F., 2016, *Frontiers of Physics*, 11, 119801 (arXiv:1601.04991)
- Melia, F., 2017a, *Frontiers of Physics*, 12, 129802 (arXiv:1602.01435)

- Melia, F., 2017b, MNRAS, 464, 1966
- Melia, F. & Abdelqader, M., 2009, IJMP-D, 18, 1889
- Melia F. and Maier R. S., 2013, MNRAS, 432, 2669
- Melia F. and Shevchuk A. S. H., 2012, MNRAS, 419, 2579
- Melia F., Wei J.-J., Wu X.-F., 2015, AJ, 149, 2
- Planck Collaboration et al., 2016, A&A, 594, id A13
- Ratnatunga K. U., Griffiths R. E., Ostrander E. J., 1999, AJ, 117, 2010
- Schwarz G. E., 1978, Ann. Statist., 6, 461
- Shu, Y., et al., 2017, ApJ, 851, 48
- Sonnenfeld A., Gavazzi R., Suyu S. H., Treu T., Marshall P. J., 2013, ApJ, 777, 97
- Sonnenfeld A., Treu T., Gavazzi R., Suyu S. H., Marshall P. J., Auger M. W., Nipoti C., 2013, ApJ, 777, 98
- Treu T., Koopmans L. V. E., 2002, ApJ, 575, 87
- Treu T., Koopmans L. V. E., 2004, ApJ, 611, 739
- Treu T., Koopmans L. V. E., Bolton A. S., Burles S., Moustakas L. A., 2006, ApJ, 640, 662
- Vishwakarma, R. G., 2013, Phys. Scr., 87, 055901
- Wei J.-J., Wu X., Melia F., 2015a, AJ, 149, 165
- Wei J.-J., Wu X., Melia F. & Maier, R. S., 2015b, AJ, 149, 102